

Valley-dependent transport in a mescoscopictwisted bilayer graphene device

Wen-Xuan Shi(史文萱), Han-Lin Liu(刘翰林), and Jun Wang(汪军)
Citation: Chin. Phys. B, 2024, 33 (**1**): 017205. DOI: 10.1088/1674-1056/acf9e4
Journal homepage: http://cpb.iphy.ac.cn; http://iopscience.iop.org/cpb

What follows is a list of articles you may be interested in

Emergence of correlations in twisted monolayer-trilayer graphene heterostructures

Zhang Zhou(周璋), Kenji Watanabe, Takashi Taniguchi, Xiao Lin(林晓), Jinhai Mao(毛金海), and Hong-Jun Gao(高鸿钧)
Chin. Phys. B, 2023, 32 (**9**): 097203. DOI: 10.1088/1674-1056/ace3a8

Tunable correlation in twisted monolayer-trilayer graphene

Dongdong Ding(丁冬冬), Ruirui Niu(牛锐锐), Xiangyan Han(韩香岩), Zhuangzhuang Qu(曲壮壮), Zhiyu Wang(王知雨), Zhuoxian Li(李卓贤), Qianling Liu(刘倩伶), Chunrui Han(韩春蕊), and Jianming Lu(路建明)
Chin. Phys. B, 2023, 32 (**6**): 067204. DOI: 10.1088/1674-1056/acc8c3

Correlated states in alternating twisted bilayer-monolayer-monolayer graphene heterostructure

Ruirui Niu(牛锐锐), Xiangyan Han(韩香岩), Zhuangzhuang Qu(曲壮壮), Zhiyu Wang(王知雨), Zhuoxian Li(李卓贤), Qianling Liu(刘倩伶), Chunrui Han(韩春蕊), and Jianming Lu(路建明)
Chin. Phys. B, 2023, 32 (**1**): 017202. DOI: 10.1088/1674-1056/ac9de4

Tunable valley filter efficiency by spin-orbit coupling in silicene nanoconstrictions

Yi-Jian Shi(施一剑), Yuan-Chun Wang(王园春), and Peng-Jun Wang(汪鹏君)
Chin. Phys. B, 2021, 30 (**5**): 057201. DOI: 10.1088/1674-1056/abcf35

Spin and valley filter in strain engineered silicene

Wang Sa-Ke (汪萨克), Wang Jun (汪军)
Chin. Phys. B, 2015, 24 (**3**): 037202. DOI: 10.1088/1674-1056/24/3/037202

SPECIAL TOPIC — Valleytronics

Valley-dependent transport in a mescoscopic twisted bilayer graphene device

Wen-Xuan Shi(史文萱), Han-Lin Liu(刘翰林)[†], and Jun Wang(汪军)

School of Physics, Southeast University, Nanjing 210096, *China*

(Received 27 June 2023; revised manuscript received 10 September 2023; accepted manuscript online 15 September 2023)

We study the valley-dependent electron transport in a four-terminal mesoscopic device of the two monolayer graphene nanoribbons vertically stacked together, where the intersection forms a bilayer graphene lattice with a controllable twist angle. Using a tight-binding lattice model, we show that the longitudinal and transverse conductances exhibit significant valley polarization in the low energy regime for small twist angles. As the twist angle increases, the valley polarization shifts to the high energy regime. This arises from the regrouping effect of the electron band in the twisted bilayer graphene region. But for relatively large twist angles, no significant valley polarization is observed. These results are consistent with the spectral densities of the twisted bilayer graphene.

Keywords: twisted bilayer graphene, valley-dependent transport, graphene nanoribbon, conductance

PACS: 72.80.Vp, 72.10.–d, 71.70.Fk **DOI:** 10.1088/1674-1056/acf9e4

1. Introduction

Over the past decade, there has been extensive and intensive research on twisted bilayer graphene (TBG) due to its fascinating properties, leading to the emergence of a new discipline called twistronics in similar van der Waals heterostructures of two-dimensional materials by controlling the relative twist angle between the two monolayers.[1–17] Near the so-called magic angle of TBG, a wide range of correlated physics has been experimentally observed, including Mott insulator,[18] superconductivity,[7,8] ferromagnetism,[19] and topology.[20–25] These exotic behaviors are closely related to the flat bands near the charge neutrality point arising from the large-scale moiré pattern. The system's properties are quite sensitive to electronic correlations and interactions when the band width is extremely narrow and the electron velocity is almost vanishing. For large twist angles, the low-energy behavior of TBG matches that of monolayer graphene, and the coherent interlayer transport is suppressed.[26,27]

Several studies[28–34] have focused on directly investigating the electronic transport of TBG using the tight-binding lattice model with arbitrary twist angles. This is because transport properties closely follow the band structure of the system and can be directly measured in experiments. Olyaei *et al.*[28] calculated the conductance of a mesoscopic TBG coupled with monolayer graphene leads and identified three qualitatively different twist angle regions: large ($\theta \gtrsim 10^\circ$), intermediate (3°–10°), and small (1°–3°) angle cases, in which the transport properties behave differently. Bahamon *et al.*[29] discovered emergent magnetic textures in a current-driven TBG system using the same numerical method when the twist angle is around the magic angle ($\theta \sim 1.05^\circ$).

In TBG, the moiré pattern can lead to the alternation of the AB and BA stackings as well as the regrouping effect of the band structure compared with the monolayer graphene, so the TBG can be employed to control the valley transport of electrons. Since a single moiré pattern can contain several thousands of atoms in the low twist angle regime, Beule *et al.*[32] employed a Wannier-like tight-binding model[35–37] to show that the TBG can produce valley-polarized electrons by use of the regrouping effect of the TBG band or Lifshitz transition with the help of an external gate voltage. The possible valley current splitter was also studied in Ref. [31] based on the zero-energy modes at the interface of the AB and BA stacking regions, which is induced by a perpendicular electric field. While the simplified tight-binding-parametrization model can capture most features of the low-energy band of moiré patterns, it may lose some topology properties of the TBG band. Therefore, it is desirable to study valley-dependent electron transport in TBG directly using the original TBG lattice model, despite the large unit cells at smaller twist angles.

In this study, we investigate valley transport in a four-terminal mesoscopic device comprised of two monolayer graphene nanoribbons vertically stacked together to form a TBG intersection with a controllable twist angle. We numerically calculate both the longitudinal and transverse conductances using the original graphene lattice model in the clean limit. Our results show that both conductances exhibit clear valley polarization, which stems from the regrouping effect of the TBG band. Valley polarization occurs in the low Fermi-energy regime when the twist angle is small, around the magic angle, and it shifts to the high energy regime as the twist angle

[†]Corresponding author. E-mail: 230228533@seu.edu.cn

© 2024 Chinese Physical Society and IOP Publishing Ltd

increases. However, for relatively large twist angles, the valley polarization becomes weak since the two layers of TBG appear to be disconnected to match the single monolayer graphene's property.

This work is organized as follows. In Section 2, we introduce a device model composed of the two single-layer graphene nanoribbons as well as the formulas for calculating the conductance. The numerical calculations of the valley-dependent conductances among different terminals are performed in Section 3 and the results are analyzed in detail. A brief conclusion is drawn in the last section.

2. Model and formula

We get started with the four-terminal mesoscopic device schematically shown in Fig. 1, where the two same monolayer-graphene nanoribbons are overlapped together and the intersection is the TBG region. The ribbon edge is chosen to be the zigzag termination here, because the wavefunctions of electrons propagating in the ribbon can be conveniently divided into two separate valleys, marked as the K or K' valley. The ribbon width is set as N representing the atom number of a transverse armchair chain or a unit slice, and the length of the ribbon is set as L denoting the armchair-chain number involved in the calculations, therefore, the total atom number in the studied 4-terminal device is $2NL$. The twist angle of the TBG is denoted as θ, with the twist axis located in the central region of the device at position $(N/2, L/2)$, where one atom in the top layer overlaps exactly over another one in the bottom layer.

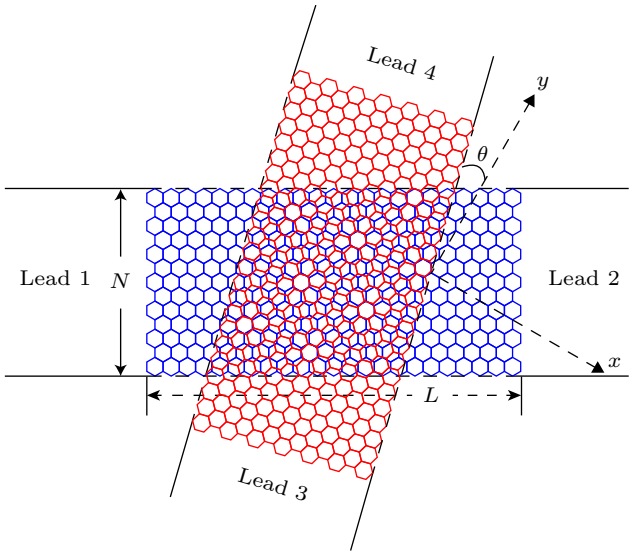


Fig. 1. Schematic of a four-terminal mesoscopic device of the two graphene nanoribbons stacked together. Four leads are assumed infinitely long and each ribbon's edge is zigzag terminated. The pristine AB stacking of the bilayer graphene is along the y-axis and θ denotes the twist angle of two layers. N and L represent the width and length of the ribbon, respectively.

A tight-binding Hamiltonian is employed to describe the device and only the p_z orbit of each C atom is assumed active

$$H = \sum_{ij} t_{ij} C_i^{\dagger} C_j, \tag{1}$$

where $C_{i(j)}^{\dagger}$ is the creation (annihilation) operator of electrons on site i (j), the hopping energies t_{ij} between carbon C, site i and j are determined by the standard Slater–Koster formula[38]

$$t_{ij} = \cos^2\phi_{ij} V_{pp\sigma}(r_{ij}) + \sin^2\phi_{ij} V_{pp\pi}(r_{ij}), \tag{2}$$

where $\cos\phi_{ij} = d_0/r_{ij}$ with $\boldsymbol{r}_{ij} = \boldsymbol{r}_i - \boldsymbol{r}_j$, and the distance-dependent Slater–Koster parameters are given by

$$\begin{aligned} V_{pp\pi}(r_{ij}) &= V^0_{pp\pi} \exp[q_\pi(1 - r_{ij}/a_0)] F_c(r_{ij}), \\ V_{pp\sigma}(r_{ij}) &= V^0_{pp\sigma} \exp[q_\sigma(1 - r_{ij}/d_0)] F_c(r_{ij}), \end{aligned} \tag{3}$$

with a smooth cutoff function $F_c(r_{ij}) = [1 + \exp((r_{ij} - r_c)/\lambda_c)]^{-1}$. Parameters[39] in the following calculations are chosen as $V^0_{pp\pi} = -2.7$ eV, $V^0_{pp\sigma} = -0.12V^0_{pp\pi}$, $a_0 = 0.144$ nm, $d_0 = 0.33$ nm, $r_c = 0.614$ nm, $\lambda_c = 0.0265$ nm, and $q_\pi/a_0 = q_\sigma/d_0 = 22.18$ nm^{-1}. The above tight-binding Hamiltonian can be simplified by limiting the inplane distance between the two neighboring sites, $r_{ij} < 2.16$ Å, so this actually limits the hopping atoms in between two monolayers of the TBG and presents an advantage that the matrix of the lattice Hamiltonian is very sparse for less time consuming in calculations. In Ref. [39], the nearly flat band near the Fermi level can be well reproduced in the vicinity of the magic angle $\theta \sim 1.1^\circ$.

In the lattice model, the valley-dependence conductance of the four-terminal device is calculated by[40]

$$g_{lm}^{\tau\tau'} = \frac{e^2}{h} T_{lm}^{\tau\tau'} = \frac{e^2}{h} \mathrm{Tr}[\Gamma_{ll}(\tau) G^r_{lm} \Gamma_{mm}(\tau') (G^r_{lm})^{\dagger}]. \tag{4}$$

Here, l (m) $= 1,2,3,4$ is the index of the different leads in Fig. 1(a), $\tau, \tau' = K$ (K') is the valley index, $T_{lm}^{\tau\tau'}$ stands for the transmission coefficient of the τ' valley electrons in the l-th lead that are transported into the τ valley in the m-th graphene ribbon lead. $G^r = [E - H_c - \sum_l \Sigma^r_{ll}]^{-1}$ is the retarded Green's function, H_c is the Hamiltonian of the scattering region of the device, E is the Fermi energy of the system, $\Gamma_{ll}(\tau) = i[\Sigma^r_{ll}(\tau) - \Sigma^{r\dagger}_{ll}(\tau)]$, the self-energy of each graphene-ribbon lead (Σ^r_{ll}) can be constituted by the left- or right-propagating electron eigenfunctions at the Fermi energy in the lth lead. Notice that only for the zigzag-edge graphene ribbon, the two valleys can directly be separated. The calculation detail of the valley-dependent $\Sigma^r_{ll}(\tau)$ of leads can be found in Ref. [40].

Despite the lack of translational symmetry in the incommensurate-structured TBG, the recursion method can still be used to calculate the Green's function G^r through the tight binding model. However, it remains challenging to divide the scattering region into the same-size block or supercell/slice even for the finite-size commensurate TBG region. Nonetheless, our main concern is the correlation function G^r_{lm}, and it

is possible to group the two slices from the l-th and m-th leads into a single block in H_c. The other components of H_c can be considered gradually when calculating G^r by the Dyson equation. Thus, the H_c can be divided into different-size blocks in a calculation-tolerable manner.

3. Result and discussion

In our numerical calculations, we set the hopping energy $t = V^0_{pp\pi} = -2.7$ eV as the energy unit, while the width of the ribbon is $N = 2048$, corresponding to a width of about 220 nm with the lattice constant $a_0 = 1.44$ Å. The length of the ribbon in the device is $L = N$, which is approximately 380 nm. The scattering region of the device comprises $N_r = 2NL$ carbon atoms. However, the atom number in the intersection region forming the TBG is slightly smaller than N_r as shown in Fig. 1, but it still contains hundreds of moiré supercells, even for a small twist angle θ.

Prior to presenting our numerical results, it is worth noting the regrouping effect of the TBG band, which arises from the electron band in the monolayer graphene Brillouin zone folded into the much smaller moiré Brillouin zone. Therefore, there are many new bands emergent due to reduction of Brillouin zone since the energy eigenvalues of electrons keep the same, and then the interaction between the two single layers gives rise to numerous emergent subbands and even the new band gaps, subsequently, the van Hove singularities in the density of states of the TBG appear at the edges of these subbands.[41–44]

We first present the valley-resolved longitudinal conductance g^K_{12} and $g^{K'}_{12}$, representing the K or K' channel conductance of lead 2 when the electrons are injected from lead 1,

$$g^\tau_{12} = \sum_{\tau'} g^{\tau'\tau}_{12}. \tag{5}$$

The longitudinal conductance is actually the monolayer graphene nanoribbon's one within the influence of an additional nanoribbon layer stacked above. The results are plotted in Fig. 2 with three typical twist angles: the small ($\theta = 2^\circ$), the intermediate ($\theta = 5^\circ$), and the large ($\theta = 30^\circ$) cases, which were classified in Ref. [28] to denote different transport regimes.

In Fig. 2(a), the conductance profiles of g^K_{12} and $g^{K'}_{12}$ show an increase linearly with the Fermi energy E, and there exist some small deviations (dips) in the relative high energy region, which are the van Hove singularities due to the regrouping effect of electron bands. In other words, the two layers are loosely coupled, especially from the standpoint of the low energy regime. Besides, the valley polarization defined by the conductance difference, $g^K_{12} - g^{K'}_{12}$, is also very low. Notice that $g^K_{12} - g^{K'}_{12} = 1(e^2/h)$ in the clean limit even for a monolayer graphene nanoribbon case, because the lowest subband of the zigzag-edge nanoribbon is only contributed by one valley conductance due to the formation of the edge state.

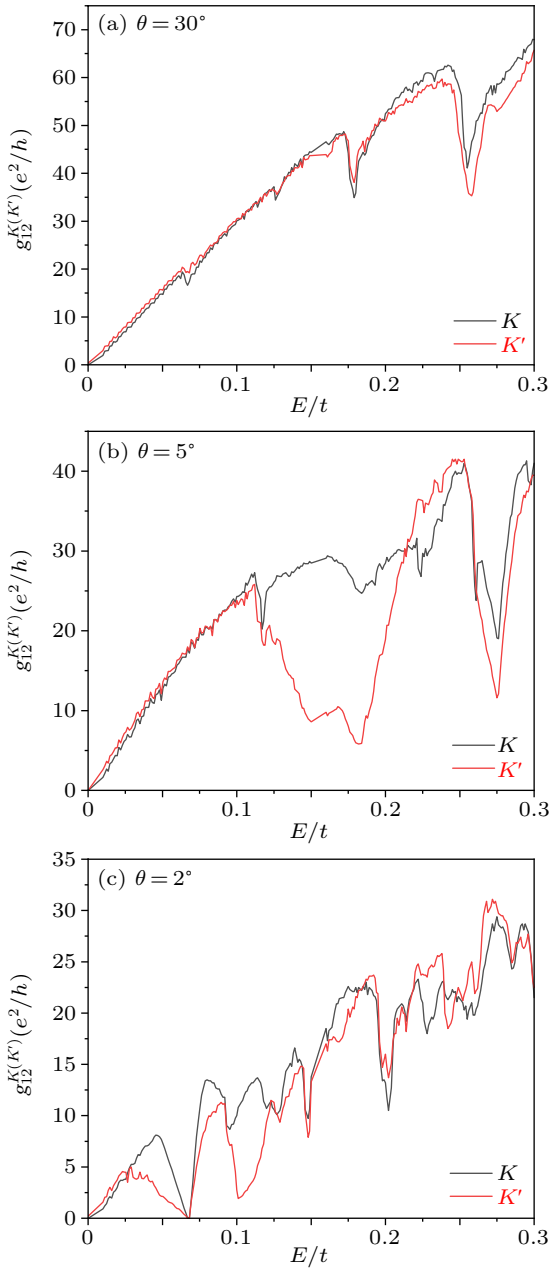


Fig. 2. Longitudinal valley-dependent conductance of g^K_{12} and $g^{K'}_{12}$ as a function of the Fermi energy E for different twist angles. Parameters are marked in each panel and described in the text.

For an intermediate twist angle $\theta = 5^\circ$, g^K_{12} and $g^{K'}_{12}$ are also depicted in Fig. 2(b). It can be seen that both of them increase linearly with E for the very low energy region but the valley polarization of $g^K_{12} - g^{K'}_{12}$ rapidly increases when $E \gtrsim 0.12t$, which is the maximum hopping energy $V^0_{pp\sigma}$ of the two layers of the TBG, indicating where is a van Hove singularity in the TBG band. This valley polarization is much more pronounced than that in Fig. 2(a), although the conductance for the large twist angle $\theta = 30^\circ$ case exhibits also a weak dip behavior. Moreover, we note that the large valley polarization shifts towards the low energy regime. Similarly, the reduction

tendency of $g_{12}^{K(K')}$ with decreasing θ indicates a shift of the energy band of the TBG towards the low energy regime.

When θ decreases further, the first van Hove singularity of the TBG band seems to be pushed to the much lower energy regime, where the nearly flat band shall develop as $1^\circ \lesssim \theta \lesssim 3^\circ$. This will result in a drastic change in the conductance landscape. Figure 2(c) shows the case for $\theta = 2^\circ$: $g_{12}^{K(K')}$ varies rapidly with E for the entire energy regime. The relationship between $g_{12}^{K(K')}$ and E deviates significantly from a linear relationship, and the conductance difference between the two valley channels is clear even for very low Fermi energy. This suggests that the two layers of the TBG are tightly coupled in comparison to Figs. 2(a) and 2(b). We note that there is a conductance zero at $E \sim 0.06t$, which reflects an energy gap in the band structure of the TBG when θ is small. This energy gap has been observed in experimental measurements[43] around $\theta = 2^\circ$.

The conductance dips in Fig. 2 generally imply that there are van Hove singularities due to the regrouping effect of the electron band, so the Lifshitz transition of the band can account for the valley polarization of the conductance, which has been already employed to produce the valley polarization in the monolayer graphene or the TBG system with the help of local potentials.[32,40] For the graphene-nanoribbon leads in our device, the valley degree of freedom is well defined but in the TBG region, other bands (or energy minimum points) arise and destroy the valley definition because it is defined as the energy minimum in the momentum space, so the valley polarization of conductance implies there should be a valley Hall effect in the system.

We also calculate the transverse conductance $g_{13}^{K(K')}$ ($g_{14}^{K(K')}$), representing the electrons injected into the device from lead 1 and collected in the K (K') channel of lead 3 (4), which are plotted in Fig. 3 for the same twist angles as in Fig. 2. For the case of large twist angle $\theta = 30^\circ$, $g_{13}^{K(K')}$ and $g_{14}^{K(K')}$ in Figs. 3(a) and 3(b) are much smaller than the longitudinal conductance $g_{12}^{K(K')}$, and even negligibly small in the low energy regime $E \lesssim 0.05t$. This is consistent with the weak coupling between the two layers for the large twist angle case, where a clear valley Hall effect is not expected to occur. For $g_{13}^{K(K')}$, there is a relatively large valley polarization in the high-energy regime, corresponding to the dips of $g_{12}^{K(K')}$ in Fig. 2(a).

Figure 3(c) shows $g_{13}^{K(K')}$ for $\theta = 5^\circ$, which increases significantly and is comparable in magnitude to $g_{12}^{K(K')}$, particularly when $E \gtrsim 0.12t$, where the valley polarization is also significant. However, in the low energy regime $E \lesssim 0.05t$, the situation remains unchanged compared to $\theta = 30^\circ$, indicating that the coupling of the two layers of TBG is stronger when the Fermi energy E is not too small. The valley polarization of $g_{13}^{K} - g_{13}^{K'}$ is substantial, suggesting the emergence of a significant valley Hall effect. Meanwhile, the transverse conductance of $g_{14}^{K(K')}$ displays a very weak valley polarization, as shown in Fig. 3(d). For small twist angle $\theta = 2^\circ$, a nearly flat band forms in the low energy regime, as reflected in the longitudinal conductance of $g_{12}^{K(K')}$ in Fig. 2(c). In Fig. 3(e), $g_{13}^{K(K')}$ is of the same magnitude as $g_{12}^{K(K')}$ when $E \lesssim 0.05t$, and the conductance difference, $g_{13}^{K} - g_{13}^{K'}$, is evident. This is consistent with the strong coupling between the two layers of TBG in the low energy regime. However, the valley polarization of $g_{14}^{K(K')}$ remains weak, as shown in Fig. 3(f).

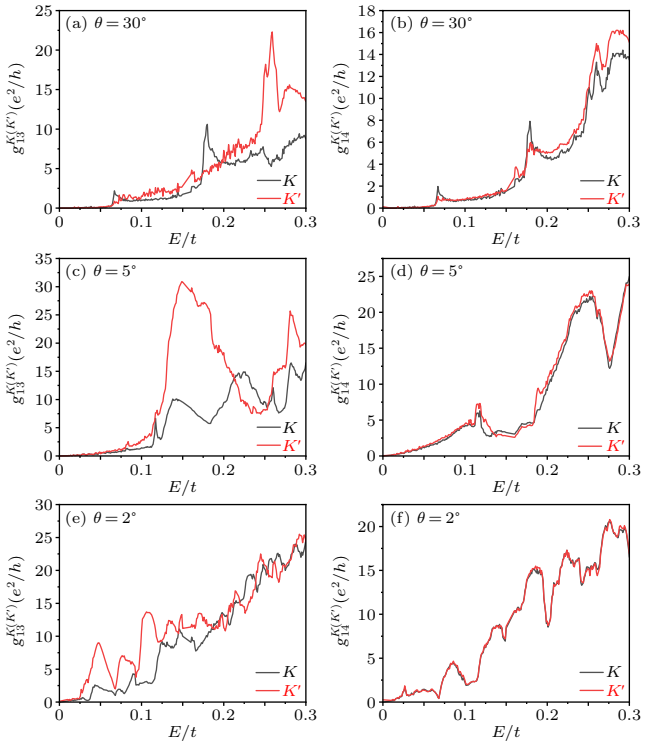


Fig. 3. Transverse valley-dependent conductance of $g_{13}^{K(K')}$ and $g_{14}^{K(K')}$ as a function of the Fermi energy E for different twist angles. Parameters are marked in each panel and described in the text.

The transverse conductances $g_{13}^{K(K')}$ and $g_{14}^{K(K')}$ are asymmetric since the device itself lacks special spatial symmetry, and the valley degree of freedom is highly dependent on the direction of current flow. In Figs. 3(e) and 3(f), there is no conductance zero, unlike the longitudinal counterpart $g_{12}^{K(K')}$ around $E = 0.06t$ in Fig. 2(c), indicating an energy gap in TBG due to the formation of the flat band in the low energy regime. However, the transverse conductances remain non-zero, suggesting that possible edge states can play a crucial role in the transverse $g_{13}^{K(K')}$ and $g_{14}^{K(K')}$ conductances in the valley Hall effect.

The conductance profiles for both transverse and longitudinal conductances exhibit rapid oscillation behaviors, owing to the presence of many bands in the small moiré Brillouin Zone, as well as many van Hove singularities. We have only calculated several incommensurate structures with $\theta = 30^\circ$,

5°, and 2°, but the commensurate structures can display similar trends with many dips or peaks in the conductance-energy dependence. Additionally, we have not shown the conductance of the hole band ($E < 0$) since the qualitative results remain the same as those presented in Figs. 2 and 3.

4. Summary

We have investigated valley transport in a four-terminal mesoscopic device consisting of two monolayer graphene ribbons stacked together, where the intersection region is the TBG with an adjustable twist angle. We numerically calculate the valley-dependent longitudinal and transverse conductances and find that significant valley polarization occurs mainly around the conductance dip where the van Hove singularity of the band exists. As the twist angle decreases, the valley polarization becomes larger and appears in much lower energy regime. In the case of relatively large twist angles, the valley polarization is shown to be quite small since the coupling of the two layers of the TBG is weak for the low energy regime.

Acknowledgment

Project supported by the National Natural Science Foundation of China (Grant Nos. 12174051 and 11874221).

References

[1] Bistritzer R and MacDonald A H 2010 *Phys. Rev. B* **81** 245412
[2] San-Jose P, Gonzalez J and Guinea F 2012 *Phys. Rev. Lett.* **108** 216802
[3] Lopes Dos Santos J M, Peres N M and Castro Neto A H 2007 *Phys. Rev. Lett.* **99** 256802
[4] Kim K, Yankowitz M, Fallahazad B, Kang S, Movva H C P, Huang S, Larentis S, Corbet C M, Taniguchi T, Watanabe K, Banerjee S K, LeRoy B J and Tutuc E 2016 *Nano Lett.* **16** 1989
[5] Sürez Morell E, Correa J D, Vargas P, Pacheco M and Barticevic Z 2010 *Phys. Rev. B* **82** 121407
[6] Lu X, Stepanov P, Yang W, Xie M, Aamir M A, Das I, Urgell C, Watanabe K, Taniguchi T, Zhang G, Bachtold A, MacDonald A H and Efetov D K 2019 *Nature* **574** 653
[7] Cao Y, Fatemi V, Demir A, Fang S, Tomarken S L, Luo J Y, Sanchez-Yamagishi J D, Watanabe K, Taniguchi T, Kaxiras E, Ashoori R C and Jarillo-Herrero P 2018 *Nature* **556** 80
[8] Cao Y, Fatemi V, Fang S, Watanabe K, Taniguchi T, Kaxiras E and Jarillo-Herrero P 2018 *Nature* **556** 43
[9] Kerelsky A, McGilly L J, Kennes D M, Xian L, Yankowitz M, Chen S, Watanabe K, Taniguchi T, Hone J, Dean C, Rubio A and Pasupathy A N 2019 *Nature* **572** 95
[10] Jiang Y, Lai X, Watanabe K, Taniguchi T, Haule K, Mao J and Andrei E Y 2019 *Nature* **573** 91
[11] Xie Y, Lian B, Jack B, Liu X, Chiu C L, Watanabe K, Taniguchi T, Bernevig B A and Yazdani A 2019 *Nature* **572** 101
[12] Sboychakov A O, Rakhmanov A L, Rozhkov A V and Nori F 2015 *Phys. Rev. B* **92** 075402
[13] Serlin M, Tschirhart C L, Polshyn H, Zhang Y, Zhu J, Watanabe K, Taniguchi T, Balents L and Young A F 2020 *Science* **367** 900
[14] Codecido E, Wang Q Y, Koester R, Che S, Tian H D, Lv R, Tran S, Watanabe K, Taniguchi T, Zhang F, Bockrath M and Lau C N 2019 *Sci. Adv.* **5** eaaw9770
[15] Huang S, Kim K, Efimkin D K, Lovorn T, Taniguchi T, Watanabe K, MacDonald A H, Tutuc E and LeRoy B J 2018 *Phys. Rev. Lett.* **121** 037702
[16] Rickhaus P, Wallbank J, Slizovskiy S, Pisoni R, Overweg H, Lee Y, Eich M, Liu M H, Watanabe K, Taniguchi T, Ihn T and Ensslin K 2018 *Nano Lett.* **18** 6725
[17] Schmidt H, Rode J C, Smirnov D and Haug R J 2014 *Nat. Commun.* **5** 5742
[18] Kim K, DaSilva A, Huang S, Fallahazad B, Larentis S, Taniguchi T, Watanabe K, LeRoy B J, MacDonald A H and Tutuc E 2017 *Proc. Natl. Acad. Sci. USA* **114** 3364
[19] Sharpe A L, Fox E J, Barnard A W, Finney J, Watanabe K, Taniguchi T, Kastner M A and Goldhaber-Gordon D 2019 *Science* **365** 605
[20] Choi Y, Kemmer J, Peng Y, Thomson A, Arora H, Polski R, Zhang Y, Ren H, Alicea J, Refael G, von Oppen F, Watanabe K, Taniguchi T and Nadj-Perge S 2019 *Nat. Phys.* **15** 1174
[21] Zhang Y H, Mao D and Senthil T 2019 *Phys. Rev. Res.* **1** 033126
[22] Bernevig B A, Song Z D, Regnault N and Lian B 2021 *Phys. Rev. B* **103** 205411
[23] Li Z, Chan H C and Xiang Y 2020 *Phys. Rev. B* **102** 245149
[24] de Paz M B, Vergniory M G, Bercioux D, Garcä-Etxarri A and Bradlyn B 2019 *Phys. Rev. Res.* **1** 032005
[25] Liu H L and Wang J 2023 *Phys. Rev. B* **107** 125412
[26] Anđelković M, Covaci L and Peeters F M 2018 *Phys. Rev. Mater.* **2** 034004
[27] Yan W, Meng L, Liu M, Qiao J B, Chu Z D, Dou R F, Liu Z, Nie J C, Naugle D G and He L 2014 *Phys. Rev. B* **90** 115402
[28] Olyaei H Z, Amorim B, Ribeiro P and Castro E V 2020 arXiv: 2007.14498
[29] Bahamon D A, Gomez-Santos G and Stauber T 2020 *Nanoscale* **12** 15383
[30] Han Y, Zeng J, Ren Y, Dong X, Ren W and Qiao Z 2020 *Phys. Rev. B* **101** 235432
[31] Hou T, Ren Y, Quan Y, Jung J, Ren W and Qiao Z 2020 *Phys. Rev. B* **102** 085433
[32] De Beule C, Silvestrov P G, Liu M H and Recher P 2020 *Phys. Rev. Res.* **2** 043151
[33] Alvarado M and Yeyati A L 2021 *Phys. Rev. B* **104** 075406
[34] Pelc M, Morell E S, Brey L and Chico L 2015 *J. Phys. Chem. C* **119** 10076
[35] Koshino M, Yuan N F Q, Koretsune T, Ochi M, Kuroki K and Fu L 2018 *Phys. Rev. X* **8** 031087
[36] Zou L, Po H C, Vishwanath A and Senthil T 2018 *Phys. Rev. B* **98** 085435
[37] Po H C, Zou L, Senthil T and Vishwanath A 2019 *Phys. Rev. B* **99** 195455
[38] Trambly de Laissardire G, Mayou D and Magaud L 2012 *Phys. Rev. B* **86** 125413
[39] Nguyen V H, Hoang T X and Charlier J C 2022 *J. Phys.: Mater.* **5** 034003
[40] Wang J J, Liu S, Wang J and Liu J F 2017 *Sci. Rep.* **7** 10236
[41] Yan W, Liu M, Dou R F, Meng L, Feng L, Chu Z D, Zhang Y, Liu Z, Nie J C and He L 2012 *Phys. Rev. Lett.* **109** 126801
[42] Ohta T, Robinson J T, Feibelman P J, Bostwick A, Rotenberg E and Beechem T E 2012 *Phys. Rev. Lett.* **109** 186807
[43] Kim Y, Herlinger P, Moon P, Koshino M, Taniguchi T, Watanabe K and Smet J H 2016 *Nano Lett.* **16** 5053
[44] Li G, Luican A, Lopes dos Santos J M B, Castro Neto A H, Reina A, Kong J and Andrei E Y 2009 *Nat. Phys.* **6** 109